Fabrication of poly (ε-caprolactone) microfiber scaffolds with varying topography and mechanical properties for stem cell-based tissue engineering applications

Junghyuk Ko, Nima Khadem Mohtaram, Farid Ahmed, Amy Montgomery, Michael Carlson, Patrick C.D. Lee, Stephanie M. Willerth, and Martin B.G. Jun

2014

http://dx.doi.org/10.1080/09205063.2013.830913

Fabrication of poly (ε-caprolactone) microfiber scaffolds with varying topography and mechanical properties for stem cell-based tissue engineering applications

Junghyuk Ko[a], Nima Khadem Mohtaram[a], Farid Ahmed[a], Amy Montgomery[a], Michael Carlson[b], Patrick C.D. Lee[c], Stephanie M. Willerth[a,d] and Martin B.G. Jun[a,*]

[a] Department of Mechanical Engineering, University of Victoria, Victoria, BC, V8W 3P6, Canada

[b] Department of Biochemistry, University of Victoria, PO Box 3055, STN CSC Victoria, BC V8W 3P6, Canada

[c] Dow Chemical Company, 2511 Midlan 433 Building, Midland, MI 48667, US

[d] Division of Medical Science, University of Victoria, Victoria, BC, V8W 3P6, Canada

Abstract.

Highly porous poly (ε-caprolactone) microfiber scaffolds can be fabricated using electrospinning for tissue engineering applications. Melt electrospinning produces such scaffolds by direct deposition of a polymer melt instead of dissolving the polymer in a solvent as performed during solution electrospinning. The objective of this study was to investigate the significant parameters associated with the melt electrospinning process that influence fiber diameter and scaffold morphology, including processing temperature, collection distance, applied voltage and nozzle size. The mechanical properties of these microfiber scaffolds varied with microfiber diameter. Additionally, the porosity of scaffolds was determined by combining experimental data with mathematical modeling. To test the cytocompatability of these fibrous scaffolds, we seeded neural progenitors derived from murine R1 embryonic stem cell lines onto these scaffolds where they could survive, migrate, and differentiate into neurons, demonstrating the potential of these melt electrospun scaffolds for tissue engineering applications.

Key words

melt electrospinning, microfibers, micro structure, scaffolds, neural tissue engineering, stem cells

[*]To whom correspondence should be addressed. Tel.:(1-250-853-3179); e-mail: mbgjun@uvic.ca

1. Introduction

Tissue engineering often uses biomaterial scaffolds that mimic the microenvironment present in healthy tissue [1, 2]. Such scaffolds should function in a manner similar to the extracellular matrix (ECM) found in normal tissue when engineering substitutes for bone, cartilage, skin, liver and nerve [3-9]. Recently, the field has focused on developing scaffolds that induce stem cells to differentiate into desired phenotypes necessary for proper tissue formation and function [8-11]. Many techniques, including particulate leaching, gas foaming, fiber bonding, solvent casting and electrospinning, have been used to fabricate scaffolds with different morphological properties [9, 12-19]. Electrospinning offers a number of advantages over these other techniques. These advantages include controlling topography and consequently tailoring the mechanical properties of electrospun scaffolds, as well as the capability to encapsulate drugs inside fibers for controlled release applications. Electrospinning can produce fibrous scaffolds with controllable porosity, sub-micron fiber size and structural homogeneity [18, 19].

Solution electrospinning requires dissolving a polymer in solvent and then applying a high voltage to this solution to induce nanofiber formation [20, 21]. Obtaining a uniform distribution of fiber sizes can be challenging when using solution electrospinning to produce nanofiber scaffolds [22]. The process of melt electrospinning involves heating up the desired polymer with the resulting melt being extruded into fibers, resulting in better reproducibility than solution electrospinning [23-25]. The melt electrospinning process does not require the use of undesirable toxic solvents for dissolving polymers like solution electrospinning does [26]. More importantly, melt electrospinning enables better control of topography compared to solution electrospinning. Pioneering works by Larrondo and Manley in the early 1980s characterized dependences of fiber diameter on the applied electrical field as well as temperature and viscosity of the polymer melt [27-29]. Additionally, other researchers characterized the mechanical and structural properties of melt electrospun fibers compared to the bulk properties of the polymer and they observed that fiber orientation influenced the bulk properties of the scaffold [30, 31].

Recent tissue engineering approaches have combined embryonic stem cells (ESCs) with biomaterial scaffolds to direct differentiation into functional tissue replacements [11]. For instance, neural tissue engineering can be used to develop therapies for reconstructing damaged nerves through the use of biomaterial scaffolds and stem cells that can mimic the microenvironment present in healthy tissue [8, 11]. ESCs are pluripotent cells, having the potential to differentiate into any cell type found in body [8]. The pluripotent nature of ESCs means they can serve as a potential cell source for virtually any tissue engineering application [32]. Many studies have successfully shown that chemical cues presented by biomaterial scaffolds can promote ESC differentiation [8, 33-35]. A similar body of work demonstrates the role of physical cues presented by scaffolds such as elasticity, micro and nanostructures of these structures can influence stem cell differentiation as well [9, 36-38]. For example, aligned nanoscale topography significantly enhanced the neuronal differentiation of ESCs [9, 39]. For electrospun fibers, these physical and mechanical factors include morphological and mechanical properties of such scaffolds, which are highly influenced by altering fiber diameter.

In this work, we used melt electrospinning to fabricate poly (ε-caprolactone) (PCL) microfiber scaffolds for ESC culture. Scaffolds made from PCL can be tailored to have different mechanical properties and

exhibit long term stability when implanted *in vivo* [40]. The purpose of this study was to analyze the parameters that influence the microfiber morphology of these scaffolds. To our knowledge, we are the first group to investigate the effect of melt electrospun microfiber diameter on the mechanical properties of the scaffolds along with their microstructure characteristics such as porosity. We determined the effect of fiber diameter on mechanical properties, such as tensile strength, the Young's modulus and strain at break, for a wide range of scaffolds as well. The influence of fiber diameter on morphological properties, such as torus volume and porosity of the scaffolds was also evaluated. Finally, ESC-derived embryoid bodies (EBs) containing neural progenitors were seeded upon the PCL microfibers to determine if these scaffolds could support stem cell culture and their neuronal differentiation. Our melt electrospun scaffolds supported cell adhesion and neuronal differentiation of ESC-derived neural progenitors. Overall, this novel combination of microfiber scaffolds and ESC-derived neural progenitors serves as a promising strategy for stem cell based tissue engineering applications.

2. Materials and Methods

2.1 Melt electrospinning setup

Poly (ε-caprolactone) (PCL) (M_n ~45,000) was purchased from (Sigma Aldrich, USA) with a melting point of 60°C. A custom-made melt electrospinning apparatus (Figure 1) consisted of a computer numerical controlled (CNC) machine (K2 CNC Inc., USA), a custom-made chamber press, a syringe pump (New Era Pump Systems Inc., USA), a heating band (Orion Telescopes Inc., USA), a custom-made machined melting chamber, a custom-made collecting drum and custom-made nozzles that could be interchanged. The flat tipped nozzles used to extrude the melt were fabricated from aluminum 6061 with internal diameters ranging from 150 to 1,700 μm (±10 μm). The custom-made nozzle was machined using a 3-axis CNC milling machine. The irradiation power used in machining the nozzles was 300 mW at a beam diameter of 3 mm. The beam was focused through a 20X microscope objective lens (Mitutoyo Co.) with a numerical aperture of 0.4. The femtosecond laser system (Spectra-Physics) operating at 800 nm with pulse duration of 120 fs and repetition rate of 1 kHz was used to produce the nozzle hole. The motion of the sample stage followed a helical path (generated using the software, GOL3D (GBC&S, France)) to ablate material from the nozzle head and cut a circular hole.

During the melt electrospinning process, 10, 15 and 20kV were applied to the molten PCL using a high applied voltage supply (Gamma High Voltage Research Inc., USA) with the working distance between the nozzle and aluminum foil collector ranging from 5 and 10cm. The PCL granules were dispensed into melting chamber with the nozzle attached and then heated to the desired temperature. The zero shear rate viscosity of PCL was measured using an ARES-G2 rheometer (TA Instruments, USA) as 291.5 Pa.sec. at 80°C using 25mm parallel plates geometry with the gap of 25mm. For the collection of randomly aligned scaffolds, a wood plate covered with aluminum foil served as the counter electrode.

2.2. Scaffold Fabrication

Parameters related to fiber diameter and morphology of scaffold when melt electrospinning include nozzle diameter, processing temperature, collection distance, applied voltage, flow rate of syringe pump and linear velocity of x and y axis in CNC machine [24, 25, 27-29, 41]. A syringe pump was mounted vertically and

connected with the heated chamber, delivering molten polymer at a flow rate of 2 mL per hour. Wood plate was covered with aluminum foil in order to make conduction as a counter electrode and the foil connected to the power supply as negative charge. The nozzle was pulled away by CNC machine controller after experiments to avoid disruption to the voltage or the flow rate.

To investigate the influence of electrical force, nozzle diameter and linear velocity were respectively fixed at 200 μm and 8.5 mm/sec. To investigate the effect of temperature, the melting chamber temperature was varied from 80°C to 120°C. Based on our parameter analysis, the melt temperature was set at 80°C with an applied voltage of 20 kV and a collection distance of 5 cm when melt electrospinning scaffolds when analyzing the effect of the varying nozzle diameter. These conditions ensured proper fiber formation during the electrospinning process. Nozzle diameters ranged in size from 150 to 1,700 μm (Table 1).

2.3 Mechanical Properties

For further analysis, 100 x 100 mm rectangular scaffolds were fabricated using CNC machine stage and then the scaffolds were cut into 100x10 mm cuboid samples. Using a micrometer (Mitutoyo, Japan), sample thicknesses were confirmed to be 2 mm. The scaffolds were confirmed for no damage during cutting by optical microscope. Conventional macro-tensile measurements were performed using an electromechanical tensile tester (Adelaide Testing Machines, Canada). All samples were mounted between holders at a distance of 5 cm. Tensile testing was conducted at a rate of 0.08mm/s at room temperature (21°C) (n=3). The amount of strain at the breaking point was calculated using the Adelaide Testing Machines software. The Adelaide Testing machine has been used for macro scale tensile testing so it would not be able to accurately measure scaffolds with thicknesses in the range of 12-220 microns. In order to measure strain accurately, the scaffolds were fabricated as the maximum thickness 2mm which was able to accumulate without any disturbances.

2.4 Analysis of Microfiber Topography

In order to manufacture a mesh of fibers, a CNC machine was used. The maximum speed of each axis is 8.5mm/s as controlled by G-code. PCL microfibers were transferred to loading stubs before carbon coating for imaging analysis. The Cressington 208 carbon was used to coat a 3nm thick carbon layer to non-conductive PCL fibers prior to scanning electron microscopy (SEM) imaging. The samples were carbon-sputtered two times for 6 seconds at 10^{-4} *m*bar. The samples were loaded in a Hitachi S-4800 field emission scanning electron microscope. High magnification images were obtained at 1 kV with an 8 mm working distance. Fiber diameters, torus diameter and overlap distance were measured using Quartz-PCI Image Management Systems® in SEM as shown in Figure 2.

2.5 Statistical Analysis

Quantitative data are presented as mean ± standard deviation (SD). The processing parameter study were screened by one-way analysis of variance (ANOVA) with the assumption of normally distributed data using Microsoft Office Excel 2010, USA; significance was defined as $p<0.05$.

2.6 Seeding of cells on PCL microfiber scaffolds

To determine suitability of scaffolds for stem cell culture, R1 (Nagy Lab) mouse embryonic stem cells were utilized. R1 cells were cultured upon mouse embryonic fibroblast feeder layers (Global stem, USA) to

maintain pluripotency [42]. R1 cells were subsequently removed from feeder layers and cultured in suspension on agar-coated plates to form embryoid bodies (EBs) for 8 days with 0.5 μM retinoic acid being added for the last 4 days to induce neural differentiation (Sigma-Aldrich) [43]. During this process, the media is changed every 2 days and the resultant EBs contains a high percentage of neural progenitor cells. Mesh electrospun scaffolds were sterilized with ultraviolent light for 30 minutes. Individual R1 EBs were removed from suspension and seeded on sterilized scaffolds. EBs were cultured on these electrospun scaffolds for 14 days before image analysis.

2.7. R1 Cells Viability Analysis

The viability of R1 EBs seeded on the scaffolds was analyzed qualitatively after 14 days using a LIVE/DEAD® Viability/Cytotoxicity Kit (Invitrogen). The kit contains a stain for viability, calcein AM, which is enzymatically converted to green fluorescing calcein by the naturally present intracellular esterase activity in live cells, and a stain for dead cells, ethidium homodimer-1, which fluoresces red upon binding to nucleic acids accessed through the ruptured cell membranes of dead cells [33]. Each well was viewed using an IncuteCyte ZOOM Essen BioScience® fluorescent microscope. Images were captured at 515 nm for green fluorescence and 635 nm for red fluorescence. Images were overlaid at layer opacity of 50%.

2.8 Immunocytochemistry and Nucleus Staining

Neuronal differentiation of R1 cells was qualitatively assessed after 14 days by immunocytochemistry targeting the neuron-specific protein β-III-tubulin. Media was removed and each well was washed with 4 mL PBS. Cells were fixed with a 10% formalin (Sigma) solution for 1 hour at room temperature and then permeabilized with 0.1% Triton-X (Sigma) solution for 45 minutes at 2 – 8 ˚C. Wells were then blocked with 5% normal goat serum (NGS, Millipore) at 2 – 8 ˚C for 2 hours. The primary antibody for β-III-tubulin (Millipore) was added to each well and incubated at 2 – 8 ˚C for up to 15 hours. Three washes with PBS were performed and the Alexafluor488-conjugated secondary antibody at a concentration of 10 μg/mL was added and incubated, protected from light exposure, at room temperature for 4 hours. Cells were washed three times with PBS to remove unbound antibody. Hoechst 33342 nucleic acid stain, 1μl in 300μl PBS was added into the last PBS wash after secondary antibody. Images were captured for green and blue fluorescence. Images were overlaid at layer opacity of 50%. Higher magnification fluorescent images were acquired on a LEICA 3000B inverted microscope using an X-cite series 120Q fluorescent light source (Lumen Dynamics) coupled to a Retiga 2000R fast cooled mono 12-bit camera (Q-imaging).

3. Simulation and Experiment Results

3.1 Effects of temperature on fiber diameter

The effects of changing the temperature of the melt from 80°C to 120°C were investigated. Figure 3(A) represents analysis of temperature and fiber diameter. Increasing temperature led to a significant increase in the fiber diameter when nozzle size was held constant. Fiber diameters were varied from 28 ± 1 μm at 80 °C temperature to 40 ± 2 μm for 120 ° C temperature (average ± SD) using 200 μm nozzle and 52 ± 4 μm at 80 °C to 58 ± 6 μm for 120 ° C using 300 μm nozzle in various temperatures.

Additionally, temperature influenced the speed of spinning fibers due to the density changes. This speed

played a key role in controlling the morphology of scaffolds. Table 2 showed fiber weights depended on temperature for 600 seconds using 200 μm nozzle. Velocity ($\frac{dl}{dt}$) of polymer extrusion was calculated by the following equation:

$$\frac{dV}{dt} = \pi r^2 \frac{dl}{dt} = \frac{1}{D}\frac{dm}{dt} \quad (1)$$

where *V* was total volume of electrospun fibers for 600 seconds, *m* was total weight of electrospun fibers, *r* was fiber radius, *t* was time of electrospinning, and density (D) of PCL polymer as a function of temperature calculated by [44]

$$\mathrm{D} = 0.9049e^{(6.392*10^{-4}*T)}/V(0,T) \quad (2)$$

where, *T* was temperature in degrees Celsius, the zero-pressure isobar *V(0,T)* equaled $A_0+A_1T+A_2T^2$ (A_0=9.9868*10^{-1}, A_1=8.1076*10^{-3}, A_2=7.0243*10^{-5} were specific constants for a given polymer [45]).

As shown in Figure 3(B), the velocities increased when temperatures increased because of low density and viscosity. The velocity was varied from 16.7 ± 6.2 to 119.5 ± 7.1mm/s ($p<0.05$) using 200 μm nozzle in various temperatures. Based on these results, morphology of scaffolds was able to be controlled variously through x and y axis speed controls.

3.2 Effects of distance applied voltage and chamber temperature on fiber diameter

Figure 4 showed the effect of distance between nozzle, counter electrode and applied voltage and chamber temperature on fiber diameter. According to Coulomb's law, magnitude of the electrical force was directly proportional to applied voltage and inversely proportional to the distance. Fiber diameter showed 49 ± 5 μm at 10kV and 28 ± 4 μm at 20kV in 5cm and 80°C. When distance was increased from 5cm to 10cm at 20kV and 80°C, fiber diameter demonstrated 49 ± 5 μm at 5cm and 93 ± 12 μm at 10cm Moreover, the diameters were changed from 49 ± 5 μm to 58 ± 3 μm when the chamber temperature was increased from 80 degree to 90 degree at 10kV applied voltage and 5cm distance. Fiber diameters increased in size by approximately 1.6 times when the collecting distance was doubled and also were increased from approximately 6% to 13% when chamber temperature was changed from 80 degree to 90 degree at different voltage and distance. However, when applied voltage was doubled, the fiber diameters decreased to half their original size.

3.3 Effects of nozzle diameter

The nozzle diameter controlled initial diameter of fibers when using direct deposition melt electrospinning. The fiber diameter then shrunk due to the electrical force and gravity after the spinning process. Figure 5 showed the relationship between nozzle diameter and fiber diameter in experiments. The fiber diameter increased from 12 ± 1 μm to 220 ± 9 μm as the nozzle diameter increased from 150 μm to 1,700 μm. The distance between nozzle and colleting plate and the voltage were respectively fixed at 5cm and 20kV in order to restrict parameters related to fiber diameter.

2 mm thick scaffolds were fabricated for testing of mechanical properties using various diameter nozzles from 150 to 1,700 μm. Depending on the fiber diameter, the resulting scaffolds contained a different number

of layers. 100 x 100 mm rectangular scaffolds were fabricated using CNC machine stage and then cut them with a sharp blade as 30 x30 mm sample. The speed of vertical and horizontal movement in CNC machine was 8.5 mm/s in the 3-axis machine. Figure 6 shows the overlapping topography depended on nozzle diameter. The overlap percentage varied from 78 ± 8 % to 20 ± 10 % as the nozzle diameter changed from 150 μm to 1,700 μm. Smaller nozzle diameter resulted in a larger overlap percentage.

3.4 Scaffold Porosity

Due to an inability to collect data on the scaffold porosity directly, we combined experimental data with the following equations to determine a theoretical porosity for the scaffolds fabricated using different nozzle sizes. The theoretical porosity was calculated based on estimation of fiber diameter, overlap area, and total volume of PCL microfibers. Figure 7(A) showed schematic mesh morphology and overlap calculation. They were assumed that the scaffold was cube-shaped, composed of perfect circular cylindrical microfibers called torus. Table 1 contained the experimental data determining the torus overlap for each scaffold based on SEM images.

The porosity of scaffold was defined by [26]

$$\emptyset_{mesh} = (1 - \frac{NV_t}{V_s}) \times 100\% \tag{3}$$

where, $\emptyset_{mesh}$, V_t, V_s, N were respectively porosity of mesh, volume of torus, volume of whole scaffold, and number of torus. The torus volume was calculated by

$$V_t = 2\pi^2 R r^2 \tag{4}$$

where, R was distance from the center of the tube to the center of the torus and r was the radius of the fiber. The volume of whole scaffold was determined by

$$V_s = w_1 w_2 H \tag{5}$$

where, w_1, w_2, H were respectively scaffold width, scaffold length, and scaffold height. The number of torus and overlap percentage was able to be calculated by

$$N = \left\{\frac{w_1}{2(R+r)}\left(1 + O_p\right)\right\}\left\{\frac{w_2}{2(R+r)}\left(1 + O_p\right)\right\}\left\{\frac{H}{4r}\right\}, O_p = \frac{A_2}{A_1} \times 100(\%) \tag{6}$$

where, O_p was overlap percentage. As shown in Figure 7(A), circle area (A_1) and overlap area (A_2) were defined by

$$A_1 = \theta R_1^2, A_2 = R_1^2\left(\theta - \frac{1}{2}\sin(2\theta)\right) + R_2^2\left(\alpha - \frac{1}{2}\sin(2\alpha)\right) \tag{7}$$

where, $\theta = \cos^{-1}(\frac{R_1^2 - R_2^2 + d^2}{2R_1 d}), \alpha = \cos^{-1}(\frac{R_2^2 - R_1^2 + d^2}{2R_2 d})$, α and θ were radian. d was a distance between two centers of circles. According to the assumption which was regular perfect circles, the radius of circles ($R = R_1 = R_2$) and the angles were same as well ($\theta = \alpha$) in Figure 7(A).

By using the parameters mentioned above, the resulting diameters of the microfibers were shown in table 1 demonstrates the result of torus parameters from SEM images. Thus, the theoretical porosity from Eq. (1) was shown in Figure 7(B) and (C). The significant factors to determine porosity were torus volume (V_t) and number of torus (N). The increment of number of torus and the decrement of torus volume were very similar from 1,700 μm to 500 μm so the Figure 7(C) showed flat in the section. However, the decrease in torus volume occurred more rapidly than the increase in the number of torus from 300 μm to 150 μm so the porosity increased.

3.5 Macro-tensile measurements

The mechanical properties including elastic modulus and strain at break were influenced by the fiber diameter. The elastic modulus decreased as the fiber diameter decreases. Nevertheless, the mechanical properties change considerably due to the wide range of fiber diameters produced (12 to 220 μm).

As fiber diameter decreased, strain at break increased as shown in Figure 8. This dependency of mechanical properties of microfibers on fiber diameter resulted from differences in breaking mechanisms. When we applied a strain on the electrospun mesh scaffolds, the scaffold elongated in the direction of displacement as they were stretched uniaxially. The scaffold composed of thicker fibers had property of higher Young's modulus and lower strain at break while the scaffold composed of thinner fibers had a lower Young's modulus and higher strain at break. For instance, an 18% decrease in fiber diameter from 220 μm to 180 μm led to an increase of almost 7% of in the strain at break and 9% of decreased in Young's modulus of fiber.

3.6 Seeding Embryoid Bodies on Microfiber Scaffolds

The ability of these microfiber scaffolds to serve as a stem cell culture substrate was examined through cell seeding experiments. ESC-derived neural progenitors adhered to these scaffolds and neuronal differentiation from seeded EBs can be observed after 14 days of culture. Figure 9 shows the results of the cell viability analysis and differentiation of neural progenitors into neurons when seeded upon melt electrospun scaffolds. Figure 9A shows a bright field image of the individual EB. Figure 9B shows the superimposed image of live and dead cells. Live cells are present in whole EBs on the scaffold. Migration of live cells along the microfibers that make up the scaffold topography was shown. Figure 9C is the same image without the phase contrast. These images verify that cells migrated from the EB along the direction of scaffold topography.

Immunostaining against the neuronal marker Tuj1 and staining using the nuclear marker Hoechst 33342 were performed after 14 days. Figures 9D and 9E show the neuronal differentiation of R1 cells with different magnification. The higher magnification image was taken using a LEICA DMI 3000B fluorescent microscope. Figure 9F shows the cell bodies based the presence of nucleus maker co-localized with the microfiber scaffold. Neurite outgrowth can be clearly seen. These images display a clear neuronal phenotype differentiated from the R1 EBs seeded on PCL microfiber scaffolds. Melt electrospinning microfibers support and direct R1 cell adhesion and can thus be seen as a suitable tool for tissue engineering.

4. Discussion

Electrospinning of polymeric fibers can be accomplished either using a polymer solution or melt to fabricate

fibers in the range of 3 nm to over 1 μm [19]. Although fabrication of microfibers through the use of solution electrospinning is possible, controlling the uniform distribution of fiber's diameter and also the architecture of scaffolds remains challenging [21]. The diameter of fibers can be manipulated by controlling the parameters of polymer solution and spinning operation. For instance, it has been shown that by changing the concentration of Polyethersulfone (PES) solution, PES fibers can be produced in the range of 283 ± 45 nm to 1452 ± 312 nm [37]. Similar to other studies of solution electrospinning [22], these results showed a poor uniform distribution of fiber diameter [37]. Yoshimoto et *al.* reported a broad fiber diameter distribution for PCL nanofibers (400nm ±200 nm) [16]. This variation in diameter may be due to the fast phase separation of PCL and the uncontrollable evaporation of volatile solvent during electrospinning. Using melt electrospinning, we could produce fibers with the average diameter of 12 ± 1μm at 80°C when using the 150 μm nozzle. A very fine fiber size distribution has been achieved for all of microfiber scaffolds produced by different nozzles. Fibers were fabricated with diameter in the range of 12 ± 1 μm to 220 ± 9 μm at 80°C. Therefore, this excellent degree of reproducibility would lead us to engineer polymeric microfibers according to the desired fiber diameter and its uniform distribution. However, it is limited to fabricate smaller fibers using melt electrospinning since flow resistance becomes dramatically high when nozzle diameter is smaller than 150 μm.

In addition to controlling fiber diameter and fiber size distribution, the other prominent property of scaffolds is controlling the architecture of scaffolds and their consequent porosity. Although there have been many studies on controlling the topography of fibers fabricated by solution electrospining, challenges remain in terms of being able to control and predict the topography of solution electrospun fibers [46]. On way to control the topography of nanofibers is using a rotating drum to collect aligned nanfoibers [18, 21]. The technique has shown limitations since the higher speed of drum would lead to induce a tensile force whish could break the nanaofibers and eventually disturbed fine control of fibers orientation [18]. Therefore, by using melt electrospinning one can control all topographical properties in a perfectly controlled way. By means of computer aided design (CAD), different structures can be fabricated [25]. Preventing fiber breakup, and bead forming, which are really tough to achieve in the case of solution electrospining, can be easily controlled by tuning melt electrospinning parameters including processing temperature, collection distance, applied voltage and nozzle size. Our on-going research is the fabrication of uniaxlialy and biaxial aligned microfiber scaffolds with very fine fiber size distribution.

Generally, the mechanical properties of electrospun fibers can be influenced by different parameters including the fiber diameter, topography and porosity, physical and chemical properties of the processed polymer such as polymer molecular weight and its distribution [31, 47]. Here, we have mainly focused on the control of fiber diameter over mechanical properties of PCL microfibers scaffolds. Our results showed that varying the porosity range from 75% to 92% lead to significant change in yield strength from 0.457 MPa to 1.886 MPA depended on nozzle diameter used to fabricate the scaffold. As expected when the fiber diameter decreased, porosity of scaffold increased and which consequently would lead to decrease in

Young's modulus. Croisier *et al.* performed the macro-tensile measurements on PCL fiber scaffolds fabricated by solution electrospinning using a higher molecular weight of PCL compared to our study [47]. Their results showed a Young′s modulus of 3.8 ± 0.8 MPa for nanofibers which is higher compared to 0.457 ± 0.042 MPa. This suggests that in addition to the fiber diameters, other parameters such as polymer molecular weight play a key role in controlling mechanical properties. According to our results, Young's modulus was varied from 0.457 MPa to 1.886 MPa, 75.77% increase, but strain at break was alternated from 12.08 mm to 6.92 mm, 42.72% decrease, when nozzle diameter was increased from 150 μm and 1,700 μm.

However, the mechanical properties are affected by a combination of many factors: porosity of fiber mat, fiber diameter, friction between fibers, thickness of fiber mat, and geometry [48]. We are able to fabricate scaffolds which have various mechanical properties in Young's modulus and strain at break.

Pluripotent stem cell lines can be differentiated into any of the specific cell lineages found in an organism, including those found in neural tissue [8, 34, 49]. One major type of pluripotent stem cells is ESCs isolated from the inner cell mass of blastocysts. One of the major challenges when differentiating pluripotent stem cells is how to control this process to produce the desired cell phenotypes. For example, when developing pluripotent stem cell therapies for the treatment of spinal cord injuries, it is desirable to produce neurons [49]. Neuronal differentiation of pluripotent stem cells can be achieved through the presentation of physical cues such as scaffold elasticity and topography [15-18, 50]. For example, aligned nanoscale topography can significantly enhance the neuronal differentiation of ESCs [16, 18]. Electrospun scaffolds fabricated by solution electrospinning have been extensively evaluated for their use in neural tissue engineering applications [18]. Our versatile technique to fabricate biocompatible microfibers via melt electrospinning provided a good degree of reproducibility to control the fiber diameter with the aim of supporting stem cell growth, adhesion, viability and neuronal differentiation. PCL electrospun microfibers have recently shown their potential for the adhesion and proliferation of human dermal fibroblasts [51]. Also it has been reported that periodontal ligament fibroblast cell can be adhered to a sheet of hybrid biomodal PCL melt and solution electrospun fibers sheet [51]. Our work combining stem cells and melt electrospun fibers demonstrates an alternative method of producing biomimetic scaffolds for neural tissue engineering applications without the need for toxic solvents. In this paper, we showed proof-of concept data that such scaffolds can be combined with ESC-derived embryoid bodies (EBs) containing neural progenitors to support stem cell culture and their neuronal differentiation. Our on-going studies will focus on quantifying the effect of topographical properties on the neuronal differentiation of ESC-derived embryoid bodies. Here, neuronal differentiation and outgrowth from EBs were observed, suggesting the influence of topography serves as a physical cue for stem cell-based tissue engineering strategies. We demonstrated, for the first time, that electrospun PCL microfibers could support the neuronal differentiation of ESC-derived neural progenitors.

5. Conclusion

While melt electrospinning, using different sized nozzles for extrusion enable fabrication of scaffolds with different fiber diameters. We can control the PCL fiber diameter by varying the processing temperature, the collecting distance and applied high voltage between nozzle and counter electrode, and nozzle diameters. This work characterizes PCL scaffolds fabricated using melt electrospinning both in terms of topography and mechanically. These scaffolds possess an open porous network with porosity ranging from 75% to 92% and yield strength from 0.457 MPa to 1.886 MPA depended on nozzle diameter used to fabricate the scaffold. As expected when the fiber diameter decreases, porosity of scaffold increases. The yield strength decreases when fiber diameter decreases, while strain at break increases when fiber diameter decreases because of flexibility. Finally these scaffolds are clearly able to support murine embryonic stem cell adhesion and differentiation, making them a useful tool for tissue engineering applications.

Acknowledgements

The authors would like to acknowledge support from Natural Sciences and Engineering Research Council (NSERC) Discovery Grants. They would also like to acknowledge the Advanced Microscopy Facility at the University of Victoria.

References

1. Griffith, L.G. and G. Naughton, *Tissue engineering--current challenges and expanding opportunities.* Science, 2002. **295**(5557): p. 1009-14.

2. Langer, R. and J.P. Vacanti, *Tissue engineering.* Science, 1993. **260**(5110): p. 920-6.

3. Davis, M.W. and J.P. Vacanti, *Toward development of an implantable tissue engineered liver.* Biomaterials, 1996. **17**(3): p. 365-372.

4. Hutmacher, D.W., *Scaffolds in tissue engineering bone and cartilage.* Biomaterials, 2000. **21**(24): p. 2529-2543.

5. Ko, J., Kolehmainen, K., Ahmed, F., Jun, M. B-G. and Willerth, SM., *Towards high throughput tissue engineering: development of chitosan-calcium phosphate scaffolds for engineering bone tissue from embryonic stem cells* American Journal of Stem Cells, 2012. **1**(1): p. 81-89.

6. Kolehmainen, K. and S.M. Willerth, *Preparation of 3D fibrin scaffolds for stem cell culture applications.* Journal of visualized experiments : JoVE, 2012(61): p. e3641.

7. MacNeil, S., *Progress and opportunities for tissue-engineered skin.* Nature, 2007. **445**(7130): p. 874-880.

8. Willerth, S.M., *Neural tissue engineering using embryonic and induced pluripotent stem cells.* Stem cell research & therapy, 2011. **2**(2): p. 17.

9. Xie, J.W., et al., *The differentiation of embryonic stem cells seeded on electrospun nanofibers into neural lineages.* Biomaterials, 2009. **30**(3): p. 354-362.

10. Martino, S., et al., *Stem cell-biomaterial interactions for regenerative medicine.* Biotechnology Advances, 2012. **30**(1): p. 338-351.

11. Willerth, S.M. and S.E. Sakiyama-Elbert, *Combining stem cells and biomaterial scaffolds for constructing tissues and cell delivery*, in *StemBook*2008: Cambridge (MA).

12. Nam, Y.S., J.J. Yoon, and T.G. Park, *A novel fabrication method of macroporous biodegradable polymer scaffolds using gas foaming salt as a porogen additive.* Journal of Biomedical Materials Research, 2000. **53**(1): p. 1-7.

13. Oh, S.H., et al., *Fabrication and characterization of hydrophilic poly(lactic-co-glycolic acid)/poly(vinyl alcohol) blend cell scaffolds by melt-molding particulate-leaching method.* Biomaterials, 2003. **24**(22): p. 4011-4021.

14. Pinto, A.R., et al., *Behaviour of human bone marrow mesenchymal stem cells seeded on fiber bonding chitosan polyester based for bone tissue engineering scaffolds.* Tissue Engineering, 2006. **12**(4): p. 1019-1019.

15. Suh, S.W., et al., *Effect of different particles on cell proliferation in polymer scaffolds using a solvent-casting and particulate leaching technique.* Asaio Journal, 2002. **48**(5): p. 460-464.

16. Yoshimoto, H., et al., *A biodegradable nanofiber scaffold by electrospinning and its potential for bone tissue engineering.* Biomaterials, 2003. **24**(12): p. 2077-2082.

17. Xie, J.W., et al., *Radially Aligned, Electrospun Nanofibers as Dural Substitutes for Wound Closure and Tissue Regeneration Applications.* Acs Nano, 2010. **4**(9): p. 5027-5036.

18. Xie, J.W., et al., *Electrospun nanofibers for neural tissue engineering.* Nanoscale, 2010. **2**(1): p. 35-44.

19. Pham, Q.P., U. Sharma, and A.G. Mikos, *Electrospinning of polymeric nanofibers for tissue engineering applications: A review.* Tissue Engineering, 2006. **12**(5): p. 1197-1211.

20. Reneker, D.H., et al., *Bending instability of electrically charged liquid jets of polymer solutions in electrospinning.* Journal of Applied Physics, 2000. **87**(9): p. 4531-4547.

21. Reneker, D.H., et al., *Electrospinning of nanofibers from polymer solutions and melts.* Advances in Applied Mechanics, Vol 41, 2007. **41**: p. 43-195.

22. Mohtaram, N.K., A. Montgomery, and S.M. Willerth, *Biomaterial-based drug delivery systems for the controlled release of neurotrophic factors.* Biomedical materials, 2013. **8**(2): p. 022001.

23. Dalton, P.D., et al., *Electrospinning of polymer melts: Phenomenological observations.* Polymer, 2007. **48**(23): p. 6823-6833.

24. Lyons, J., C. Li, and F. Ko, *Melt-electrospinning part I: processing parameters and geometric properties.* Polymer, 2004. **45**(22): p. 7597-7603.

25. Dalton, P.D., et al., *Direct in vitro electrospinning with polymer melts.* Biomacromolecules, 2006. **7**(3): p. 686-690.

26. Park, S.H., et al., *Development of dual scale scaffolds via direct polymer melt deposition and electrospinning for applications in tissue regeneration.* Acta Biomaterialia, 2008. **4**(5): p. 1198-1207.

27. Larrondo, L. and R.S.J. Manley, *Electrostatic Fiber Spinning from Polymer Melts .3. Electrostatic Deformation of a Pendant Drop of Polymer Melt.* Journal of Polymer Science Part B-Polymer Physics, 1981. **19**(6): p. 933-940.

28. Larrondo, L. and R.S.J. Manley, *Electrostatic Fiber Spinning from Polymer Melts .2. Examination of the Flow Field in an Electrically Driven Jet.* Journal of Polymer Science Part B-Polymer Physics, 1981. **19**(6): p. 921-932.

29. Larrondo, L. and R.S.J. Manley, *Electrostatic Fiber Spinning from Polymer Melts .1. Experimental-Observations on Fiber Formation and Properties.* Journal of Polymer Science Part B-Polymer Physics, 1981. **19**(6): p. 909-920.

30. Pedicini, A. and R.J. Farris, *Mechanical behavior of electrospun polyurethane.* Polymer, 2003. **44**(22): p. 6857-6862.

31. Lee, K.H., et al., *Mechanical behavior of electrospun fiber mats of poly(vinyl chloride)/polyurethane polyblends.* Journal of Polymer Science Part B-Polymer Physics, 2003. **41**(11): p. 1256-1262.

32. Vats, A., et al., *Embryonic stem cells and tissue engineering: delivering stem cells to the clinic.* Journal of the Royal Society of Medicine, 2005. **98**(8): p. 346-350.

33. Willerth, S.M., et al., *The effects of soluble growth factors on embryonic stem cell differentiation inside of fibrin scaffolds.* Stem cells, 2007. **25**(9): p. 2235-2244.

34. Lopez-Gonzalez, R. and I. Velasco, *Therapeutic Potential of Motor Neurons Differentiated from Embryonic Stem Cells and Induced Pluripotent Stem Cells.* Archives of Medical Research, 2012. **43**(1): p. 1-10.

35. Li, W., K. Jiang, and S. Ding, *Concise review: A chemical approach to control cell fate and function.* Stem cells, 2012. **30**(1): p. 61-8.

36. Engler, A.J., et al., *Matrix elasticity directs stem cell lineage specification.* Cell, 2006. **126**(4): p. 677-689.

37. Christopherson, G.T., H. Song, and H.Q. Mao, *The influence of fiber diameter of electrospun substrates on neural stem cell differentiation and proliferation.* Biomaterials, 2009. **30**(4): p. 556-564.

38. Keung, A.J., et al., *Rho GTPases mediate the mechanosensitive lineage commitment of neural stem cells.* Stem cells, 2011. **29**(11): p. 1886-97.

39. Mahairaki, V., et al., *Nanofiber Matrices Promote the Neuronal Differentiation of Human Embryonic Stem Cell-Derived Neural Precursors In Vitro.* Tissue Engineering Part A, 2011. **17**(5-6): p. 855-863.

40. Dash, T.K. and V.B. Konkimalla, *Poly-epsilon-caprolactone based formulations for drug delivery and tissue engineering: A review.* Journal of Controlled Release, 2012. **158**(1): p. 15-33.

41. Subramanian, C., et al., *The melt electrospinning of polycaprolactone (PCL) ultrafine fibers.* Polymer-Based Smart Materials - Processes, Properties and Application, 2009. **1134**: p. 229-234.

42. Qiang-Sun Zheng, D.-B.O., Xiong-Tao Liu and Jing-Jing Guo, *Maintaining Embryonic Stem Cells and Induced Pluripotent Stem Cells, Embryonic Stem Cells: The Hormonal Regulation of Pluripotency and Embryogenesis*April, 2011: IN TECH. 672.

43. Bain, G., et al., *Embryonic Stem-Cells Express Neuronal Properties in-Vitro.* Developmental Biology, 1995. **168**(2): p. 342-357.

44. Haynes, W.M., *the CRC Handbook of Chemistry and Physics* 93RD Edition, 2012. **Chemical Rubber Company**.

45. Ronald P. Danner, M.S.H., *Handbook of Polymer Solution Thermodynamics.* Design Institute for Physical Property Data (DIPPR), American Institute of Chemical Engineers, 1993.

46. Huang, Z.M., et al., *A review on polymer nanofibers by electrospinning and their applications in nanocomposites.* Composites Science and Technology, 2003. **63**(15): p. 2223-2253.

47. Croisier, F., et al., *Mechanical testing of electrospun PCL fibers.* Acta Biomaterialia, 2012. **8**(1): p. 218-224.

48. Liao, T.Y., S. Adanur, and J.Y. Drean, *Predicting the mechanical properties of nonwoven geotextiles with the finite element method.* Textile Research Journal, 1997. **67**(10): p. 753-760.

49. Willerth, S.M. and S.E. Sakiyama-Elbert, *Cell therapy for spinal cord regeneration.* Advanced Drug Delivery Reviews, 2008. **60**(2): p. 263-276.

50. Oh, S., et al., *Stem cell fate dictated solely by altered nanotube dimension.* Proceedings of the National Academy of Sciences of the United States of America, 2009. **106**(7): p. 2130-2135.

51. Paul D. Dalton, C.V., Brooke L. Farrugia, Tim R. Dargaville, Toby D. Brown and Dietmar W. Hutmacher, *Electrospinning and additive manufacturing: converging technologies.* Biomaterials, 2013. **1**: p. 171-185.

Table 1.

Microstructure of scaffolds fabricated at 80°C. (All data presented as the mean (n=3) ± the standard deviation)

Nozzle diameter(μm)	*Fiber diameter(μm)*	*Overlap percentage(%)*	*r(μm)*	*R(μm)*
1,700	220±9	30.1±1.2	110	1,600±60
1000	180±7	35.2±1.3	90	1,300±40
838	132±5	40.1±1.6	66	1,100±40
741	100±4	50.3±2.0	50	1,020±40
500	82±3	57.0±2.3	41	800±30

300	52±4	65.1±2.6	26	710±30
200	28±1	70.4±2.8	14	620±20
150	12±1	80.2±3.2	6	510±10

Table 2.

PCL fiber properties depended on temperatures (spinning time: 10minutes using 200 μm nozzle) (n=3)

Temperature(°C)	80	90	100	110
Weight(g)	0.11±0.03	0.32±0.05	0.72±0.04	1.18±0.06
Fiber diameter(μm)	28±1	31±1	33±1	37±1
Density(g/cm^3)[44]	0.4542	0.4172	0.3840	0.3543

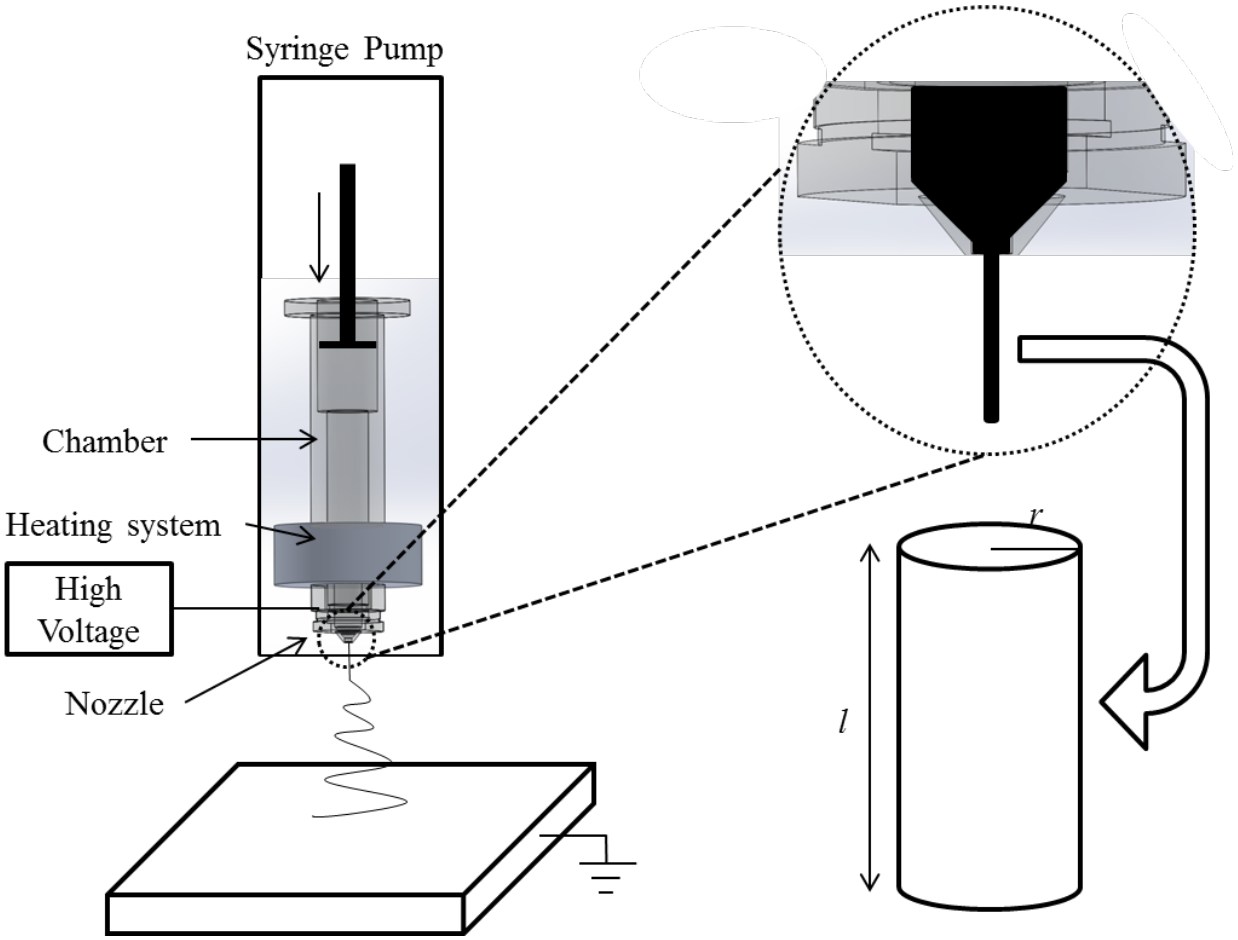

Figure 1. Schematic of custom-built melt electrospinning device.

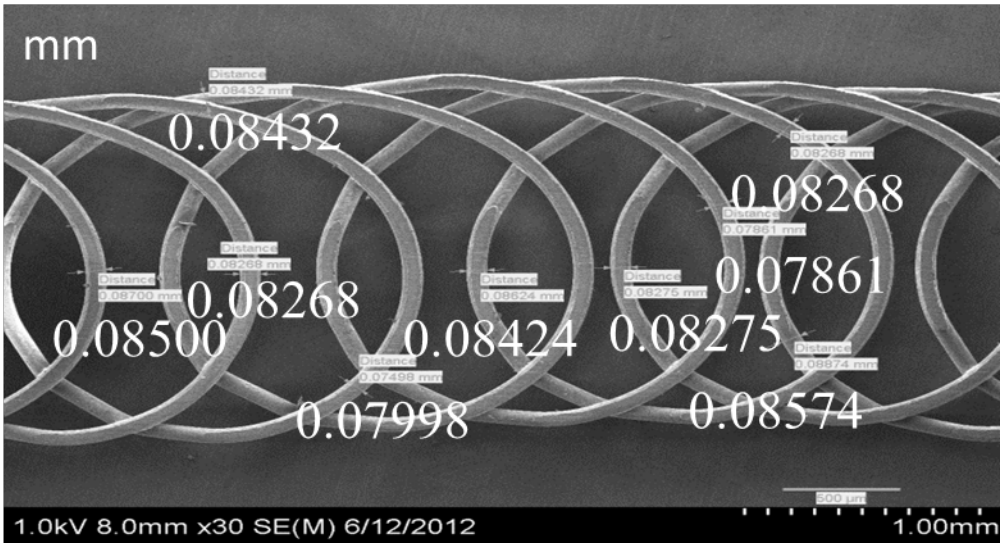

Figure 2. Scanning electron microscopy of PCL scaffolds, measuring fiber diameter using Quartz-PCI Image Management Systems® when using 500 μm nozzle at 5cm collecting distance.

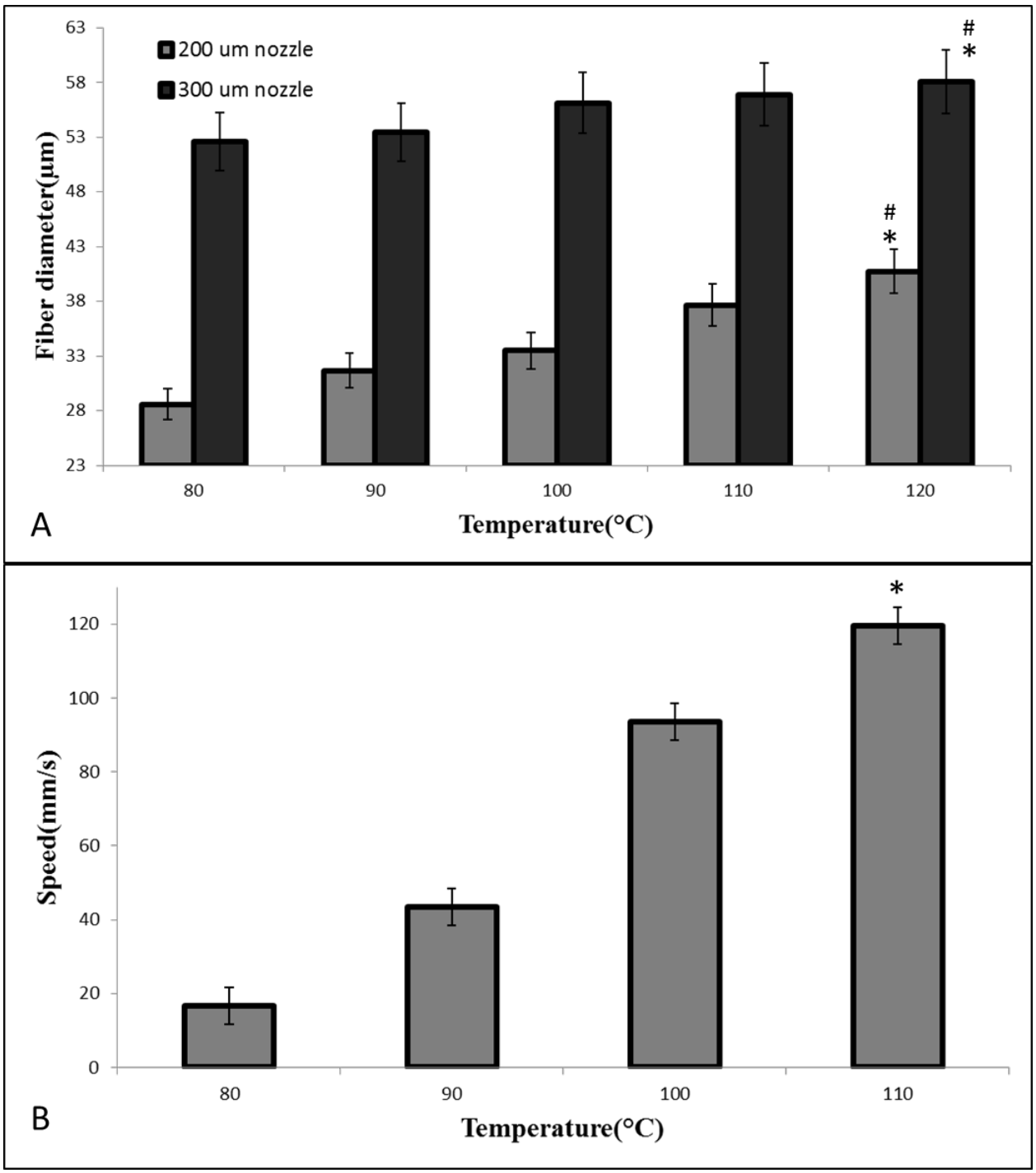

Figure 3. A) The effect of temperature on the resulting fiber diameter and (B) The effect of temperature on speed of polymer extrusion under various temperatures using 200 µm nozzle. (n=3 for both studies) * indicates $p<0.05$ versus all other temperatures. # indicates $p<0.05$ versus the other nozzle in each temperatures.

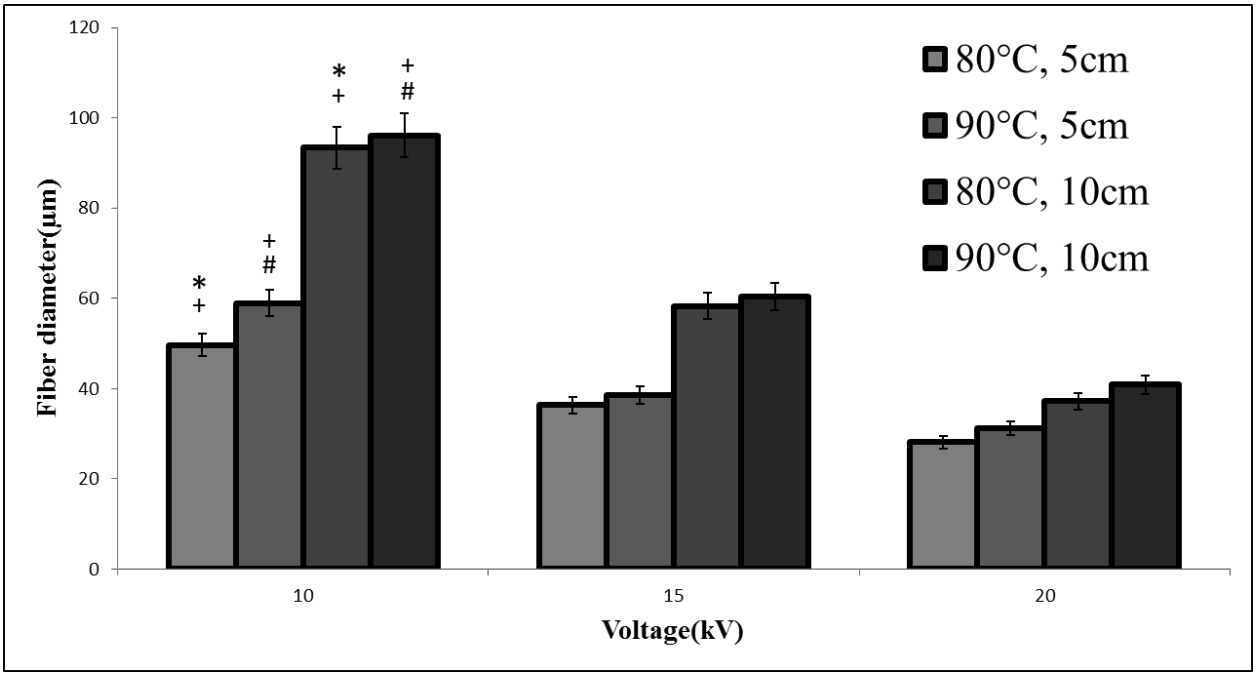

Figure 4. The effects of collection distance, temperature and applied voltage on the resulting fiber diameter using 200 μm nozzle (n =3), * indicates $p<0.05$ versus other distance at 80°C. # indicates $p<0.05$ versus other distance at 90°C. + indicates $p<0.05$ versus all other voltages.

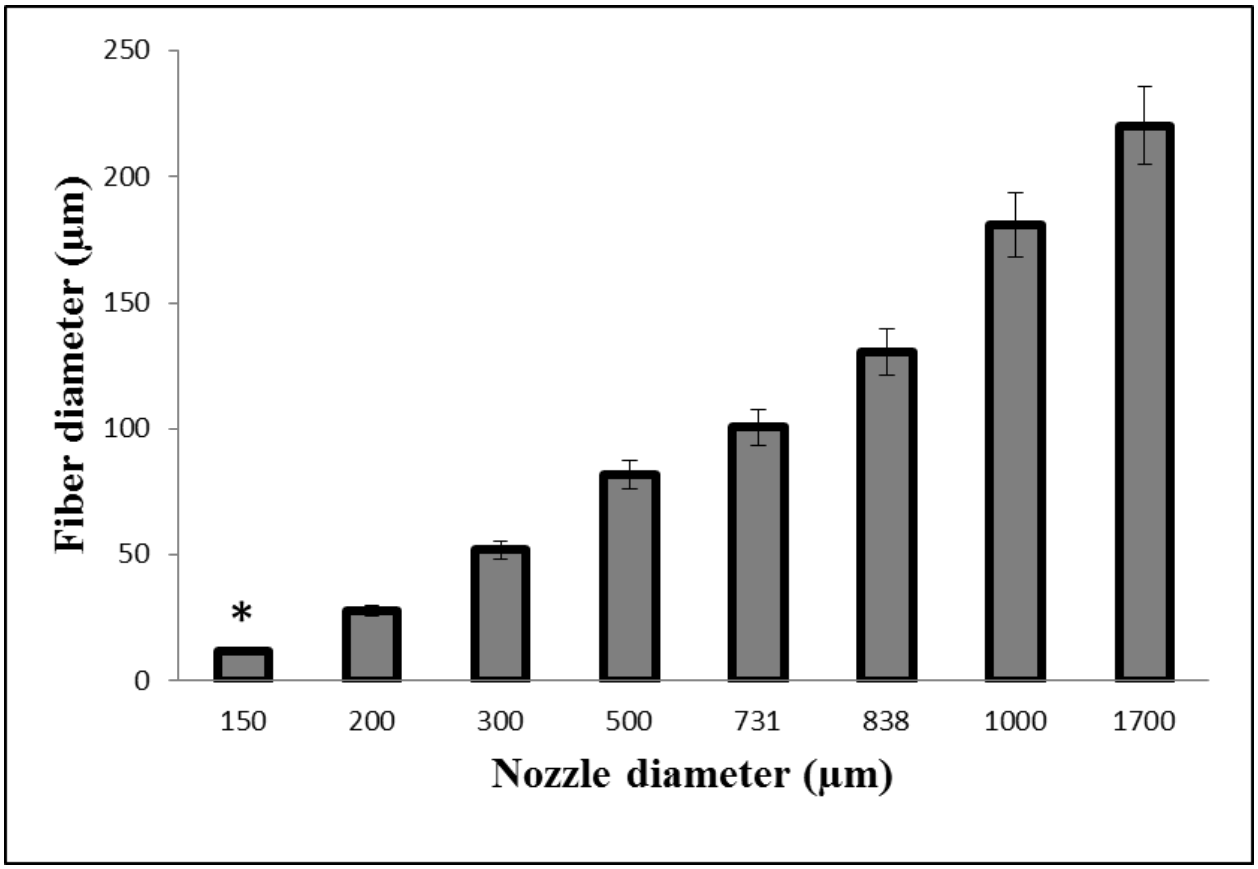

Figure 5. The effect of nozzle diameter on fiber diameter when melt electrospinning process occurs at 5cm distance, 20kV voltage, and 80°C. (n=3) * indicates $p<0.05$ versus all other nozzles.

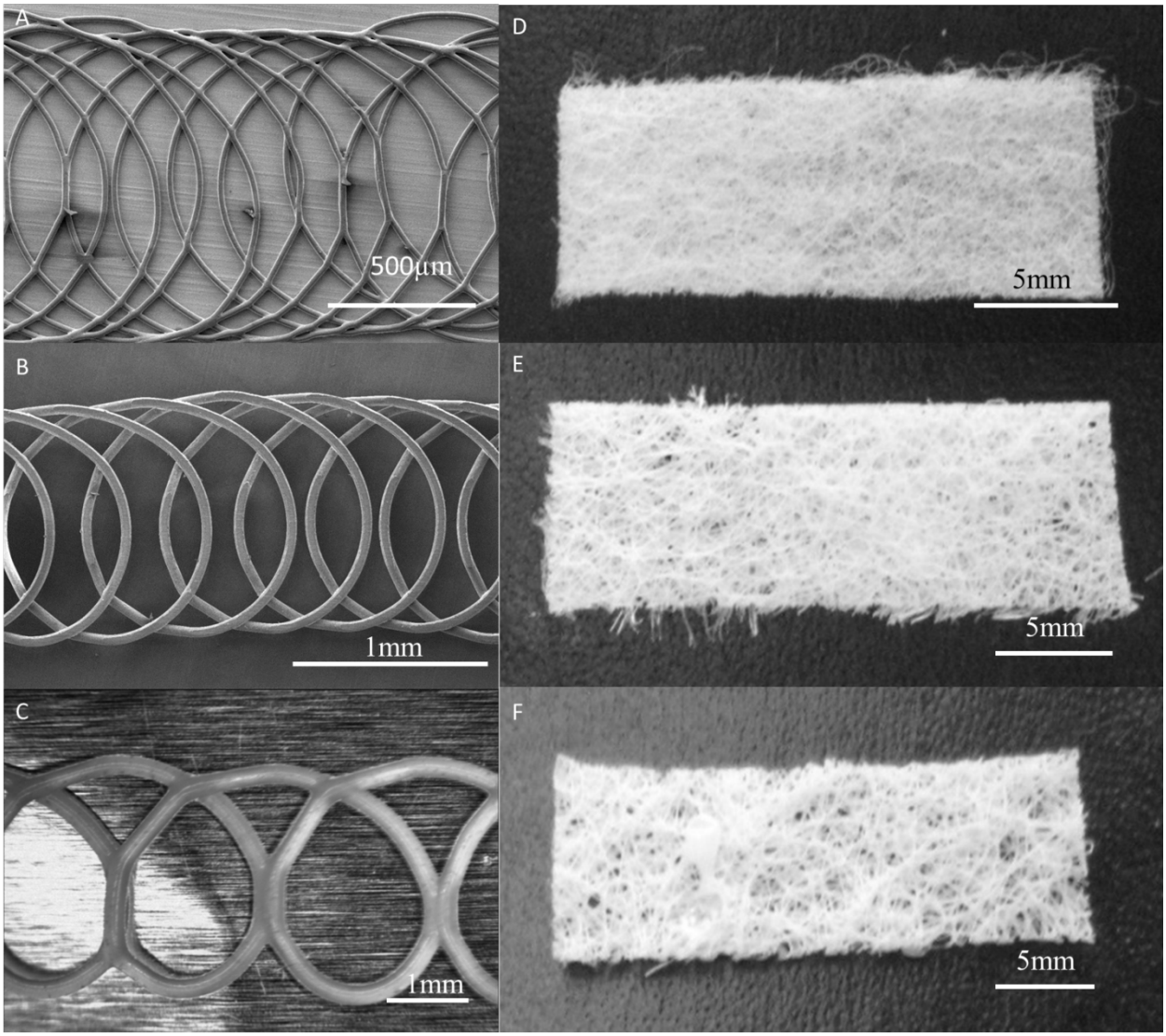

Figure 6. SEM images, optical microscope image and digital camera images of coiled loop microfiber depended on nozzle diameters at 80°C, 5cm, and 20kV; (A)-(D) 12μm diameter using 150 μm nozzle, (B)-(E) 82 μm diameter using 500 μm nozzle, and (C)-(F) 220 μm using 1,700 μm nozzle. (n=3)

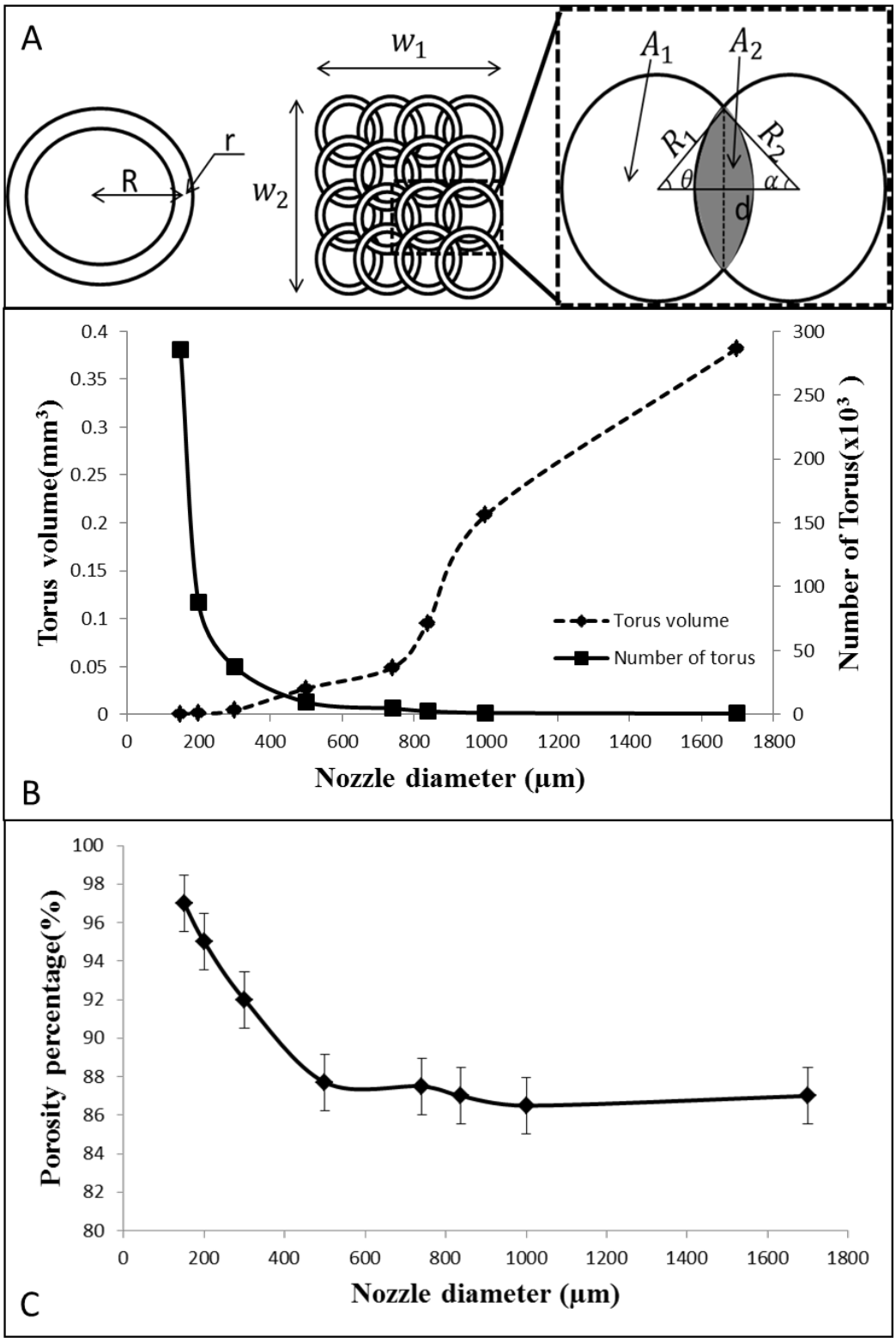

Figure 7. (A) A schematic showing the mesh morphology produced by melt electrospinning and how the degree of overlap was calculated, (B) Torus volume and Number of Torus in various nozzle diameter, (C) Theoretical porosity of scaffolds.(n=3)

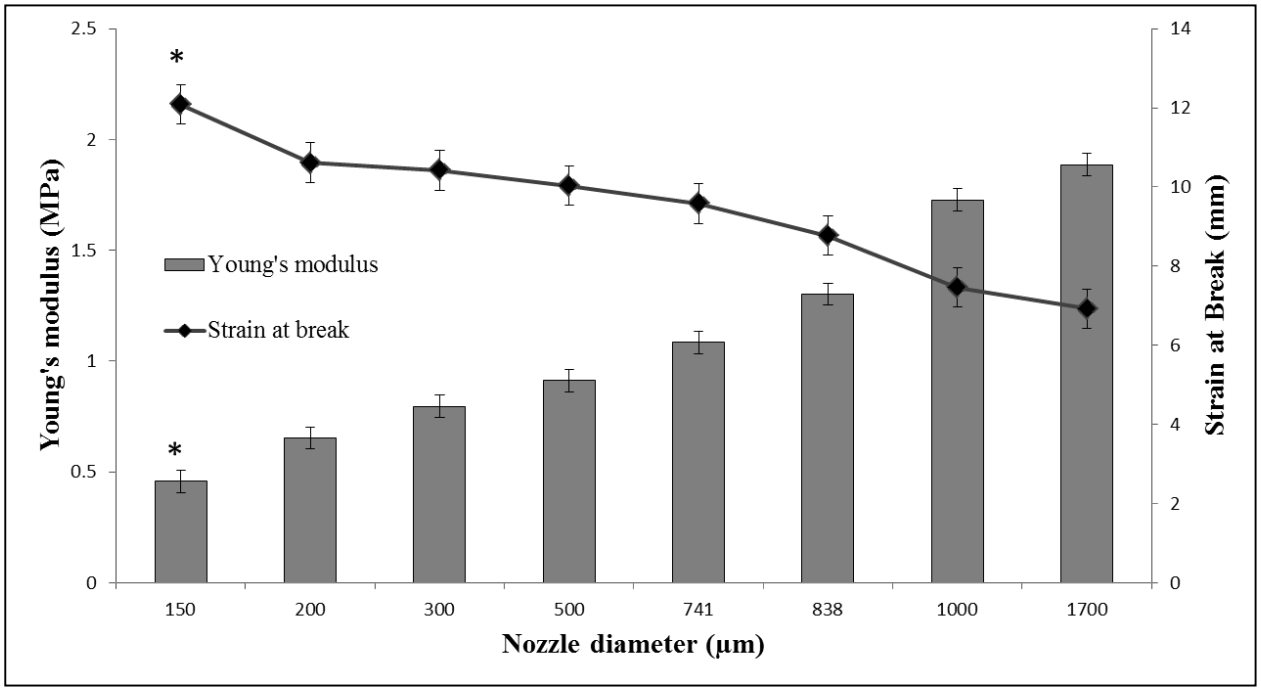

Figure 8. Mechanical properties of microfiber scaffolds using various nozzles (n=3), * indicates $p<0.05$ versus other nozzle diameters.

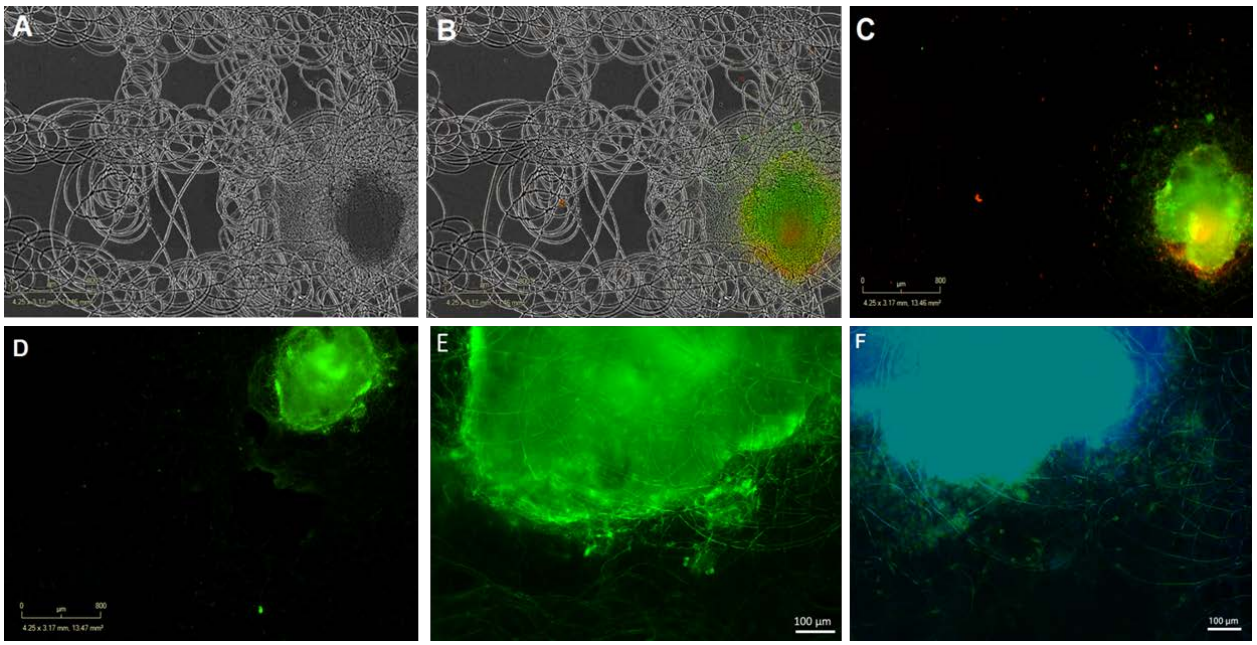

Figure 9. Live/dead analysis and differentiation of neural progenitors into neurons when seeded upon melt electrospun scaffolds after 14 days of culture. A) Bright field image. B) Superimposed image of live and dead cells over the phase contrast image. C) Superimposed image of live and dead cells without the phase contrast image superimposed. Scale bars represent 800µm. D and E) Immunohistochemistry performed on R1 EBs after 14 days of culture on mature cell marker Tuj1 expressed by neurons. F) Superimposed image of Tuj-1 and Hoechst

33342 nuclear marker. A 0.200 mm nozzle was used for fabricating a mesh scaffold at 80°C, 5cm, and 20kV.